ISSN 1070-4272, Russian Journal of Applied Chemistry, 2009, Vol. 82, No. 7, pp. 1164−1171. © Pleiades Publishing, Ltd., 2009.
Original Russian Text © A.V. Korshunov, A.P. Il'in, 2009, published in Zhurnal Prikladnoi Khimii, 2009, Vol. 82, No. 7, pp. 1068−1075.

INORGANIC SYNTHESIS AND INDUSTRIAL INORGANIC CHEMISTRY

Oxidation of Copper Nanopowders on Heating in Air

A. V. Korshunov and A. P. Il'in

Tomsk Polytechnical University, Tomsk, Russia

Received December 22, 2008

Abstract—The morphology and structure of copper nanopowders produced by electrical explosion of conductors are considered. The regularities of nanopowder oxidation in air were studied during linear and isothermal heating. The characteristics of initial powders in relation to the kinetic oxidation parameters were determined and the dependence of phase composition of the products of nanopowder oxidation on the heating conditions and dispersity of initial powders was found.

DOI: 10.1134/S1070427209070039

Submicrometer- and nano-sized copper powders are widely used for preparation of nanostructured functional materials [1]. The above materials have aroused interest because of their properties, which are markedly different from the properties of materials produced from coarse commercial powders.

Copper possesses high oxygen affinity and oxidizes to form Cu_2O even at temperatures on the order of 100°C and under the partial oxygen pressures ~10^{-5} mm Hg [2]. Copper oxidation at higher temperatures and pressures yields a mixture of oxides, Cu_2O and CuO, whose relative content in the reaction products is determined by state and purity of a metal and by environmental conditions [3–6]. Products of high-temperature oxidation of compact copper [3, 5–8] and thin copper films [9] formed at varied partial oxygen pressures have been studied in sufficient detail. As known [5, 6], the oxide CuO is a product of Cu_2O oxidation. CuO formation is possible above a certain critical thickness of a Cu_2O layer on the metal surface and impossible below a certain limiting partial pressure of oxygen (13.3 kPa [5]). Virtually no CuO is present in the oxide layer on copper at low temperatures (below 150°C) [5]. In the temperature range 300–500°C, the oxide layer contains 4–10 wt % CuO, on the average, depending on P_{O_2}; at $t > 800$°C the CuO content is virtually pressure-independent [6].

A low-temperature (below 500°C) oxidation of copper in relation to phase composition of the products and oxidation kinetics is less well understood; experimental data concerning this problem are often controversial and unambiguously explained [10–13]. From the literature, data on the oxidation of highly dispersed copper powders are lacking.

In this work, the regularities of oxidation of preliminarily passivated copper nanopowders heated in air were studied depending on their characteristics and heating conditions.

EXPERIMENTAL

We used in the study copper nanopowders (CNPs) produced by electrical explosion of conductors (EEC). The EES method consists in evaporating a conducting wire of certain length under the action of high power electrical pulse (current density as high as 10^{10} A m^{-2}). The dispersity of the nanopowders thus obtained depends on the energy supplied to a conductor, conductor characteristics, and pressure of an inert gas in explosion chamber [14]. The CNPs obtained were passivated in argon in a controlled flow of air to avoid heating and subsequent sintering of the sample. The passivated powders were kept in conventional hermetic containers. The CNPs nos. 1–3, used in the study, were obtained in 1999 and CNPs nos. 4 and 5, in 2007 (Table 1). In the test experiment, we used a coarse PMS copper powder (particle size about 40 μm) and analytically pure grade copper oxide Cu_2O.

The morphology of the samples and the elemental composition of a surface layer of the CNP particles were

Table 1. Characterization of copper powders used in the study

Sample no.	Explosion voltage, kV	Particle diameter, nm	Data for 1999		Data for 2007	
			Specific surface area, $m^2 g^{-1}$	Weight fraction of copper, %	Specific surface area, $m^2 g^{-1}$	Weight fraction of copper, %
1	18	200–1300	3.9	88.1	6.9	67.5
2	26	130–1050	8.2	85.4	16.8	57.3
3	30	110–500, 800–4000	10.2	79.0	14.2	53.6
4	24	220–1200	–	–	4.1	88.5
5	28	120–1300	–	–	9.0	87.5
6	PMS	–40000	–	–	0.01	97.5

studied with a JSM-5500 scanning electron microscope (SEM) equipped with an EDX microanalyzer. The size distribution of CNP particles in ethylene glycol was determined with the means of a Nanosizer ZS instrument (Malvern); the measurement range was 0.6 nm–6 μm. The specific surface area of the CNP samples was calculated by the BET method from a low-temperature adsorption of nitrogen. The composition and structure of the surface oxide layer of CNP particles was examined under a JEM-3010 high-resolution transmission electron microscope (JEOL); accelerating voltage was 300 kV. The state and composition of the oxide layer of particles was investigated by the Fourier transform IR spectroscopy (a Nikolet 6700 FTIR spectrometer).

The phase composition and structure of the initial powders were determined by X-ray diffraction (DRON-3M diffractometer, $Cu_{K\alpha}$ radiation). The quantitative content of crystalline phases in the samples was estimated by comparing results of the X-ray phase analysis (XPA) with the Reference Intensity Ratio (RIR) [15]. The lattice parameters of the metal copper were determined by the full-profile analysis of the diffraction patterns [15].

The regular features of copper powder oxidation in air were studied by differential thermal analysis (SDT Q 600 analyzer). 10–20-mg samples were placed into corundum crucibles preliminarily calcined to 1500°C. The temperature in the furnace was increased to 1200°C at a linear rate of 5 and 10 deg min^{-1}. The change in the sample mass was recorded to within 0.1 μg and the accuracy in measuring temperature by BET method was 0.001°. The data of the thermogravimetry (TG) were used to calculate the kinetic oxidation parameters and determine the content of metal copper in the initial samples. The products of the powder oxidation under isothermal conditions were obtained after calcining samples in a muffle furnace preliminarily heated to certain temperature. The phase composition of the intermediate oxidation products formed under the conditions of linearly increased temperature was identified by XPA.

The characteristics of the CNPs nos. 1–5 stored for different times are listed in Table 1 along with those of a coarse PMS powder (no. 6).

The nanopowders used in the study were in the form of 5–20-μm agglomerates. The shape of the CNP particles formed by electroexplosion is close to spherical. Under the non-equilibrium conditions realized at high EES voltages, the CNPs characterized by the bimodal particle-size distribution are formed. Samples obtained at low EES voltages are polydispersed, have the broad particle-size distribution, and contain larger portion of coarse particles (Table 1).

The content of metal copper in freshly prepared CNPs is 90–95 wt %; for powders stored for 1–3 years this value decreases to 85–88% (Table 1). The residue is oxides and adsorbed substances. According to the data of the elemental analysis, the NP samples contain up to 0.25 wt % of iron as major impurity. According to the X-ray phase analysis of the CNPs studied, a major crystalline phase is a metal copper with the face-centered cubic lattice, whose parameter exceeds a conventional value by 0.2% on the average. The Scherrer method gave an average value of 35 nm for crystallite size in freshly prepared powders and larger value after storage.

A necessity to passivate CNPs leads to the presence of certain content of copper oxides. The oxide layer in the samples stored for no more than 1 year has a thickness on the order of 5–10 nm and consists of Cu_2O of the cuprite

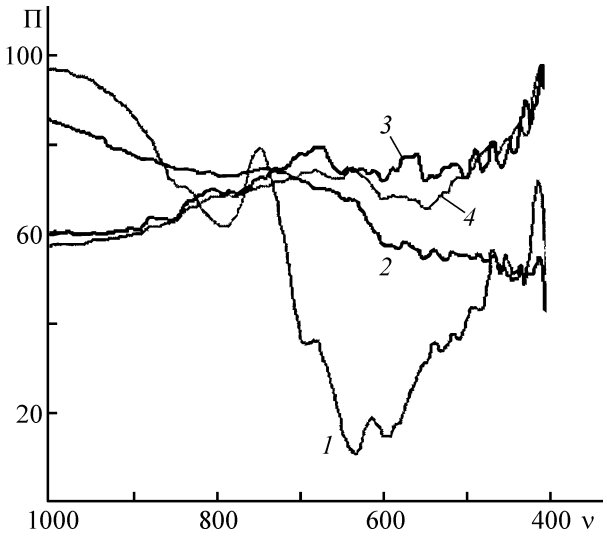

Fig. 1. The IR spectra of copper oxides and copper nanopowders. (*T*) Transmission (%) and (ν) wave number (cm^{-1}). (*1*) Cu_2O, (*2*) CuO, (*3*) CNP no. 3, and (*4*) CNP no. 4.

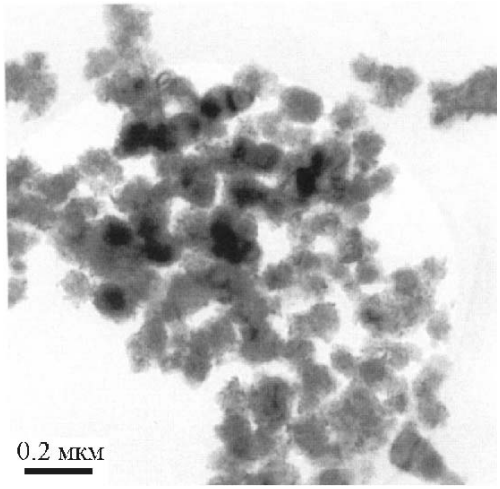

Fig. 2. TEM images of CNP particles (sample no. 3).

structure. The thickness of the oxide layer stored for about 3 years increases to 30–35 nm, with crystalline CuO of the tenorite structure present in the NP oxide layer along with Cu_2O. The most oxidized is sample no. 3 (Table 1). The oxide layer of powders nos. 1–3 constitutes a mixture of Cu_2O and CuO and that of powders nos. 4–6, Cu_2O. The XPA of the CNP samples revealed somewhat lower content of the oxides, in comparison with DTA, which shows that the oxide layer on the particle surface is to a certain extent amorphous. The content of Cu_2O and CuO on the outer part of the oxide layer is different for different samples and depends on the NP dispersity. For example, the IR spectrum of sample no. 3 has a series of

Table 2. Composition of the oxide layer on the surface of CNP particles

CNP no.	Face symbol (hkl)	Interplanar spacing, nm		Reference
1	111	0.2323	0.233	CuO
3	111	0.2524	0.253	CuO
	200	0.2311	0.231	CuO
	111	0.2465	0.246	Cu_2O
	111	0.2524	0.253	CuO
	002	0.2531	0.253	CuO

weak absorption bands in the wave number region 443–603 cm^{-1}, that corresponds to similar bands in the Cu_2O spectrum (Fig. 1) [16, 17]. In the spectrum of sample no. 4, these bands are absent. At the same time, a broad absorption band within 580–600 см$^{-1}$, that is typical of CuO spectrum and is virtually absent in the spectrum of sample no. 3, is present. The microdiffraction analysis (high resolution TEM) of the particle surface layer also revealed Cu_2O and CuO, with the Cu_2O content in CNPs with larger fraction of fine particles larger (Table 2).

The analysis of the photomicrographs of the CNP samples stored for a long time shows that copper particles of certain minimal sizes (80–150 nm) are completely oxidized on storage and contain no metal core (Fig. 2). The XPA and TEM analyses of the oxide layers revealed nanosized crystals of copper oxides. Because the oxidation of copper particles causes volume to increase considerably (the Cu, Cu_2O, and CuO molar volumes are 7.2, 23.6, and 12.3 mol cm^{-3}, respectively), joints of the crystallites formed in the course of the oxidation have low mechanical strength and easily disintegrate under external exposure (shaking and pouring a powder from one container into another).This explains why after prolonged storage the specific surface area of CNP samples increases by more than a factor of 1.5 (Table 1). Disintegration of the oxide layer in CNP suspensions is also observed. In this case, the system consists of 10–15-nm colloidal copper oxide nanocrystals, which makes it possible to characterize CNP state in solutions by electrochemical methods [18].

Copper oxides are known to differ in thermal stabilities: Cu_2O melts without decomposition at 1242°C and CuO decomposes at 1026°C [19]. Along with this, the equilibrium partial oxygen pressure over these oxides

even at relatively low temperatures (500–800°C) is comparatively large [6]. To evaluate a possible effect of oxides' decomposition on the behavior of the TG curves, we calculated the equilibrium partial oxygen pressures for various temperatures. The thermal decomposition of copper oxides can proceed by equations:

$$Cu_2O \leftrightarrows 2Cu + 1/2O_2, \quad (1)$$

$$CuO \leftrightarrows Cu + 1/2O_2, \quad (2)$$

$$2CuO \leftrightarrows Cu_2O + 1/2O_2. \quad (3)$$

We used in the calculations the thermodynamic data of [20]; the temperature was varied within 300–1350 K. The logarithm of the equilibrium partial oxygen pressure as a function of temperature was calculated by formula:

$$\log P_r = \frac{2\left[\Delta_r H_{298} + \int_{298}^{T} \Delta_r C_p dT - T\left(\Delta_r S_{298} + \int_{298}^{T} \frac{\Delta_r C_p}{T} dT\right)\right]}{2.3RT},$$

where P_T is equilibrium partial oxygen pressure at temperature T; $\Delta_r H_{298}$, $\Delta_r S_{298}$, and $\Delta_r C_p$ are changes in the enthalpy, entropy, and isobaric heat capacity, respectively, in the course of reaction; R is the universal gas constant**.** All values are given in the International System of Units (SI).

The $\log P_{O_2} = f(T)$ graphs for reactions (1)–(3) are plotted in Fig. 3.

Upon decomposition of copper oxides, P_{O_2} approaches atmospheric pressure at 930°C (Fig. 3). In this case, the main pathway for decomposition must by reaction (3), which agrees with a value of t_{decomp} for CuO. The calculated P_{O_2} value for reaction (3) at 1030°C is 357 Pa, which is approximately 60 times lower than in air and corresponds to a 0.35 % degree of the oxide decomposition. The decomposition of the oxide CuO onto simple substances [reaction (2)] can occur above 1030°C, with this process less profitable than the reaction yielding Cu_2O and oxygen. The results of the calculation show that Cu_2O decomposition onto simple substances [reaction (1)] is thermodynamically impossible up to a melting temperature of copper (1083°C [19]) (see Fig. 3). The data presented show that in the thermogravimetric analysis the loss of mass by CNP samples upon decomposition of copper oxides, products of Cu oxidation, within 100–1030°C may be neglected.

The conversion degree α of the samples was determined from data of the thermal analysis and the oxidation rate $v = d\alpha/d\tau$ was calculated from differential of α with respect to time.

The thermograms of the PMS powder no. 6 and CNP no. 4 recorded during linear heating at a rate of 10 deg min^{-1} in air are demonstrated in Fig. 4. The DTA data show that the reactivities of the given samples differ markedly. About 1.5-wt % gain of mass by PMS sample owing to oxidation is observed even at low temperatures (25–220°C).

The oxidation of PMS sample is intense within 220–620°C ($\Delta m/m_0 = 24.58\%$). In the given temperature interval the TG curve can be conventionally divided onto three sections (Fig. 4). Within 220–270°C the process rate rapidly increases to 0.0053 min^{-1}, with mass gain 4%. As temperature is increased further up to 460°C, the oxidation rate slightly increases to 0.0072 min^{-1} ($\Delta m/m_0$=18%). In the temperature range 470–500°C the rate of the PMS oxidation increases again, attaining a maximum value of 0.0097 min^{-1} at 500°C. On further heating to 550°C, the oxidation rate decreases and at 560°C the sample mass does not virtually change. The DTA curve has exothermic peaks with flat maxima in the given temperature regions.

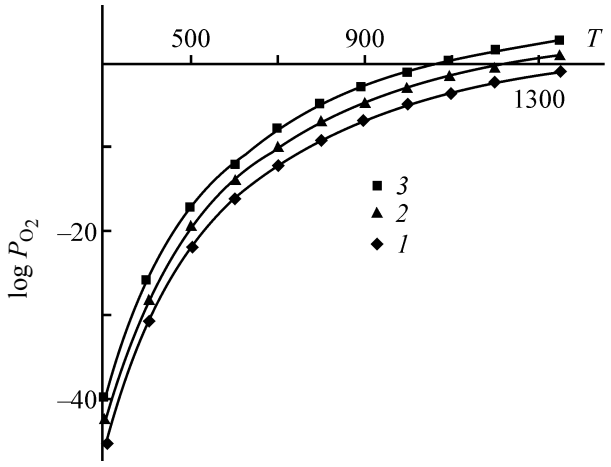

Fig. 3. The calculated dependences of the logarithm of equilibrium partial oxygen pressure P_{O_2} on temperature T (K) for decomposition of copper oxides by reactions (1)–(3).

Table 3. The oxidation parameters for copper nanopowders and copper oxide Cu_2O obtained during linear heating in air

Sample no.	Explosion voltage, kV	Particle diameter, nm	Data for 1999		Data for 2007	
			Specific surface area, $m^2\ g^{-1}$	Weight fraction of copper, %	Specific surface area, $m^2\ g^{-1}$	Weight fraction of copper, %
1	18	200–1300	3.9	88.1	6.9	67.5
2	26	130–1050	8.2	85.4	16.8	57.3
3	30	110–500, 800–4000	10.2	79.0	14.2	53.6
4	24	220–1200	–	–	4.1	88.5
5	28	120–1300	–	–	9.0	87.5
6	PMS	–40000	–	–	0.01	97.5

The study of the phase composition of the products formed in PMS oxidation during linear heating showed that the oxide Cu_2O is formed in the temperature range 220–270°C. In the 270–470°C range, Cu_2O and CuO are formed simultaneously. At 560°C, the oxidation of Cu_2O to CuO is complete.

The relative content of Cu_2O and CuO in the oxidation products formed under isothermal heating for 1.5 h agrees with that obtained during linear heating. According to the XPA data (see Fig. 5), the oxide Cu_2O is major product of the PMS oxidation at 250°C, Cu_2O and CuO at a mass ratio of about 1.4 are present simultaneously at 350°C, metal copper is absent at 450°C, with the above mass ratio in the oxidation product approximately 1:1.15. The oxidation product of PMS heated at 500°C for 1.5 h is CuO with trace amounts of Cu_2O.

The regular features of the CNP oxidation are different from those of PMS. All CNP samples are characterized by an about 0.4% mass loss within 25–185°C. This finding may be explained by desorption of gases and water vapors from the surface with a high S_{sp} value, which is very typical for highly dispersed systems [14]. Another distinction consists in a pronounced multistep character of the oxidation observed during linear heating of samples. The thermograms of the CNP oxidation have two oxidation peaks spaced by 80–100°C (Fig. 6). The parameters of the CNP oxidation depend on the powder characteristics and heating rate (Table 3). A major mass gain for sample no. 4, approximately as high as 14%, is within 190–350°C (Figs. 4, 6). The range 190–245°C corresponds to the first oxidation stage. The maximum oxidation rate in this stage exceeds that of PMS oxidation within 220–270°C by a factor of 5.8. According to the XPA data, this stage corresponds to CNP oxidation with the formation of Cu_2O.

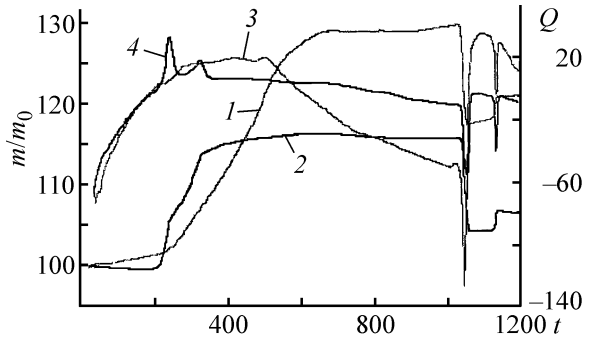

Fig. 4. Thermograms of PMS and CNP powders obtained by heating at a rate of 10 deg min^{-1} in air. (m/m_0) mass loss (%), (Q) thermal effect (mW), and (t) temperature (°C). Curve: (*1, 2*) TG; (*3, 4*) DTA. Powder: (*1, 3*) PMS and (*2, 4*) CNP no. 4.

The second stage of the CNP oxidation proceeds in the temperature range 270–350°C. The maximum rate v_{max} in this stage is twice lower than in the first stage. The phase analysis of the CNP oxidation product formed during linear heating to 350°C confirmed formation of CuO. The comparison of the above data with those for PMS oxidation shows that a coarse powder is oxidized with simultaneous formation of CuO and Cu_2O in a broader temperature range, 250–560°C.

The first and the second stages of the CNP oxidation are spaced by a region of temperatures, wherein the oxidation rate is low (about 0.005 min^{-1}).

To substantiate the specificity of the chemism of the copper powder oxidation, we studied the behavior of the Cu_2O reagent during heating in air within the same range of temperatures (Table 3). The low rate of the reaction

$$Cu_2O + 1/2O_2 = 2CuO, \quad (4)$$

and relatively high temperatures of the Cu_2O oxidation, compared to the parameters of CNP oxidation in the second stage, may be due to the size and structure effects. As was shown above, the oxide Cu_2O, product of low-temperature oxidation of nanopowders, consists of small-size crystallites, which are responsible for its better reactivity.

The Newkirk estimate [21] of the effective activation energy $E_{a,eff}$ of the oxidation stages based on results of the TG analysis obtained on heating of CNP samples at a rate of 5 deg min^{-1} gave the values of 156 ± 5 and 54 ± 3 kJ mol^{-1} for the first and second oxidation stages, respectively [reaction (4)]. Note, the $E_{a,eff}$ value of the CNP oxidation found from the TG curve within 430–540°C and that of the Cu_2O oxidation within 480–550°C are 50 kJ mol^{-1}, on the average. Virtual coincidence of the $E_{a,eff}$ values for oxidation of Cu_2O and copper nanopowders, along with the data of the XPA, confirm proceeding of the reaction (4) in the above temperature regions.

The value of $E_{a,eff}$ for the first stage of CNP oxidation is close to the activation energy E_a of diffusion of the Cu^+ cations in the cuprite lattice (151 kJ mol^{-1} [6]). The nonlinearity of the $\ln(\Delta m/m_0)$–$1/T$ dependence makes estimate of $E_{a,eff}$ of CNP oxidation within 220–430°C improbable. Virtual coincidence of the $E_{a,eff}$ values for the first stage of the CNP oxidation and E_a of Cu^+ diffusion confirm proceeding of reaction (4) in this stage and is consistent with the generally accepted conclusion that metal copper oxidizes with the formation of Cu_2O [5, 6].

The experimentally observed sequence of the CNP oxidation stages during linear heating may be explained by the size effect. After attaining a certain temperature, particles on the order of 100 nm in size undergo complete $Cu \rightarrow Cu_2O$ oxidation for relatively short time. A further increase in the temperature causes $Cu_2O \rightarrow CuO$ process to proceed. In this case, the content of the residual metal copper in CNP is determined by the content of coarse particles, which oxidize considerably slower. This conclusion is confirmed by the DTA of CNP samples obtained by electrical explosion at low voltages and containing considerable fraction of coarse particles. In the first turn, numerical predominance of coarse particles in the sample makes temperature range, wherein oxidation proceeds, broader. For example, sample no. 1 (Table 1) is oxidized within 205–600°C, with mass gain 16%;

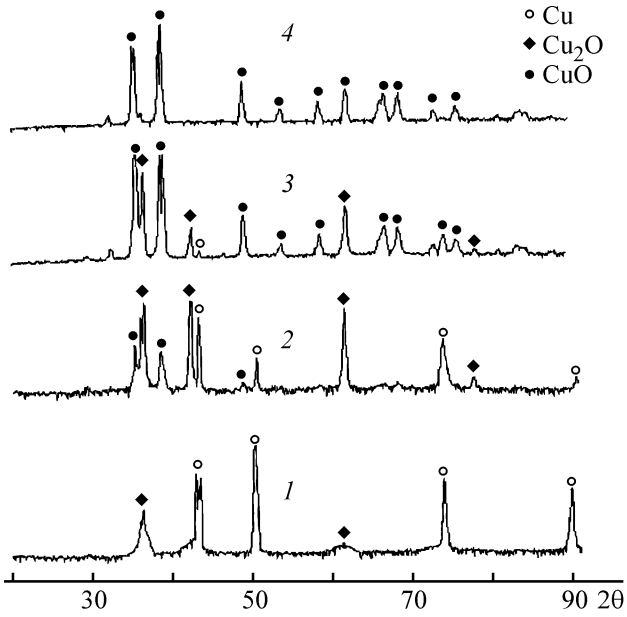

Fig. 5. X-ray diffraction patterns of the oxidation products formed on heating of PMS samples for 1.5 h at different temperatures in air. (2θ) Bragg angle (deg). Temperature (°C): (*1*) 250, (*2*) 350, (*3*) 450, and (*4*) 500.

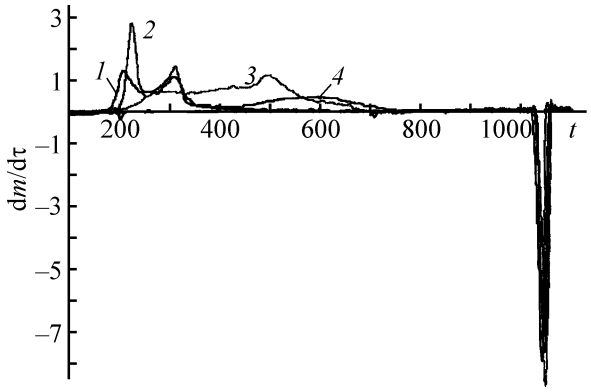

Fig. 6. DTG curves obtained for oxidation in air at a heating rate of 10 deg min^{-1}. ($\Delta m/m_0$) mass change (mg min^{-1}) and (t) temperature (°C). (*1*) CNP no. 3, (*2*) CNP no. 4, (*3*) PMS, and (*4*) Cu_2O.

The limiting mass gain (17.2%) is attained at 675°C. The v_{max} is attained at 325°C and makes 0.010 min^{-1} (Table. 3). In the given case, the DTA cannot clearly distinguish between the oxidation steps. Apart from this, the oxidation product formed at higher temperatures also contains residual copper. Thus, under otherwise the same conditions, the reactivity of samples is determined by their dispersity. Sample no. 1 in dispersity and oxidation parameters occupies the intermediate place between samples nos. 3, 4, on the one side, and PMS samples, on the other side.

The oxidation degree of the initial CNPs stored for different times exerts certain effect on the oxidation parameters obtained during heating in air. The data of Table 3 show that in the presence of oxide film on the surface of CNP particles stored for a long time the temperature of the onset of the oxidation somewhat decreases in comparison with the case of particles stored for a short time. In this case, the temperature, at which the oxidation rate at the first stage is maximal, somewhat decreases too. The corresponding temperature at the second stage is virtually the same for samples stored for different times.

For all the samples studied, the thermal decomposition of CuO formed upon complete oxidation is intense above 1000°C (Fig. 6). The process proceeds at virtually the same temperature for all samples (1029°C on the average). The experimentally observed temperature of the CuO decomposition is in good agreement with a reference value [19]) and the results of the thermodynamic calculations and does not depend on the dispersity of initial powders and heating conditions. For all samples, the mass loss is virtually the same (9.8%), close to a theoretical value of 10.0% for reaction (3). It is necessary to note that the temperature, at which CuO decomposition is complete, is also virtually the same for all samples (1058°C on the average).

CONCLUSIONS

(1) Copper nanopowders produced by electrical explosion differ from coarse powders by larger reactivity with respect to oxidation in air. The nanoparticles of the powders stored for more than 2–3 years in conventionally hermetic containers oxidize completely. Complete oxidation of coarse PMS powder is attained at 620°C and that of nanopowders, at 400°C, with the conditions of the linear heating the same (10 deg min^{-1}). The temperatures of the onset of the oxidation for PMS and nanopowders are close (220 and 180°C, respectively, on the average). Increasing the storage time of the nanopowders decreases the temperature of the onset of their oxidation.

(2) Results of the thermogravimetric analysis showed that the nanopowders oxidize in two stages spaced by 80–100°: at the first stage copper oxidizes to Cu_2O and at the second stage, the oxide Cu_2O oxidizes to CuO. The rate of the first stage correlates with the fraction of nanoparticles in the powder. The effective energies of activation of the stages were determined to be 156 ± 5 and 54 ± 3 kJ mol^{-1}, respectively. A multistep character of the oxidation as a whole and the low energy of activation of the second stage are accounted for by the size effect.

(3) The phase composition of the oxidation products obtained under isothermal heating of copper powders is determined by the dispersity of initial sample under otherwise the same conditions. At the same sintering time (1.5 h), the residual copper is present in the products of PMS oxidation to 450°C, with Cu_2O and CuO fractions at this temperature comparable. In the products of nanopowder oxidation, residual copper at 350°C was not found, with CuO a dominating phase at this temperature.

(4) The results obtained can be used for the development of attestation system for metal nanopowders.

ACKNOWLEDGMENT

The study was financially supported by the Russian Foundation for Basic Research (project no. 08-08-12077-ofi).

REFERENCES

1. Pool, Ch. P., and Owens, F.G., *Introduction in Nanotechnology*, New York: Wiley, 2003.
2. Vasilevich, A.A., Shpiro, G.P., Alekseev, A.M., et al., *Kinet. Katal*., 1975, vol. 16, no. 6, pp. 1571–1577.
3. Pilling, N.B., and Bedworth, R.W., *J. Inst. Met*., 1923, vol. 29, pp. 529–591.
4. Shishakov, N.A., Andreeva, V.V., and Andrushchenko, N.K., *Stroenie i mechanism obrazovaniya okisnykh plenok na metallakh* (The Structure and Mechanism of Formation of Oxide Films on Metals), Moscow: Akad. Nauk SSSR, 1959.
5. Hauffe, K., *Reaktionen in und an Festen Stoffen*, Berlin: Springer, 1955.
6. Kubaschewsky, O., and Hopkins, B.E., *Oxidation of Metals and Alloys*, London: Butterworths, 1962.
7. Vinogradov, V.M., and Prisedskii, V.V., *Vopr. Khim. Khim. Tekhn*., 2003, no. 6, pp. 39–42.
8. Zhu, Y., Mimura, K., Hong, S.-H., and Isshiki, M., *J. Electrochem. Soc*., 2005, vol. 152, no. 8, pp. 296–301.
9. Fromhold, A.T., and Anderson, M.H., *Oxidation of Metals,* 2004, vol. 62, pp. 237–272.
10. Njeh, A., Wieder, T., and Fuess, H., *Surf. Interface Anal.,* 2002, vol. 33, pp. 626–628.
11. Emel'yanova, T.A., and Semenova, A.S., *Izv. Vyshch.*

Uchebn. Zaved., Tsvet. Metal., 2005, no. 5, pp. 48–55.

12. Chen, Ch., Yamaguchi, T., Sugawara, K., and Koga, K., *J. Phys. Chem. B.*, 2005, vol. 109, pp. 20669–20672.
13. Borisova, N.V., Surovoi, E.P., and Titov, I.V., *Izv. Tomsk. Politekh. Univ*., 2006, vol.309, no. 1, pp. 86–90.
14. Il'in, A.P., and Tikhonov, D.V., *Fiz. Khim. Obrab. Mater.*, 2002, no. 6, pp. 60–62.
15. Rusakov, A.A., *Rentgenografiya metallov* (X-Ray Diffraction Analysis of Metals), Moscow: Atomizdat, 1977.
16. Tsuge, A., Uwamino, Y., and Ishizuka, T., *Analyt. Sci.*, 1990, vol.6, pp. 819–822.
17. Papadimitropoulos, G., Vourdas, N., Vamvakas, V., and Davazoglou, D., *J. Phys.: Conf. Ser.,* 2005, vol. 10, pp. 182–185.
18. Korshunov, A.V., and Il'in, A.P., *Fiz. Khim. Obrab. Mater.*, 2007, no. 3, pp. 70–75.
19. *Spravochnik khimika* (Chemist's Reference Book), Nikol'skii, B.P., Ed., Leningrad: Goskhimizdat, 1963, vol. 2.
20. *Kratkii spravochnik fiziko-khimicheskikh velichin* (Concise Reference Book on Physicochemical Constants), Ravdel', A.A., and Ponomareva, A.M., Eds**.,** Leningrad: Khimiya, 1983.
21. Wendlandt, W., *Thermal Methods of Analysis*, New York: Wiley, 1974.